Journal of Materials Chemistry C

PAPER

View Article Online
View Journal



Cite this: DOI: 10.1039/c7tc03023a

# Ultrafast photoresponse organic phototransistors based on pyrimido[4,5-*g*]quinazoline-4,9-dione polymer†

Jesse T. E. Quinn,[a] Fezza Haider,[a] Haritosh Patel,[a] Daid A. Khan,[a] Zhi Yuan Wang[b] and Yuning Li*[a]

Received 6th July 2017,
Accepted 8th August 2017

DOI: 10.1039/c7tc03023a

rsc.li/materials-c

We report the photoresponse characteristics of a pyrimido[4,5-*g*]quinazoline-4,9-dione (PQ) based polymer, **PPQ2T-BT-24**, which served as an active channel layer in organic phototransistors (OPTs). OPTs using this polymer showed very short rise time of 3 ms and fall time of 59 ms, photoresponsivity (*R*) of 0.24 and external quantum efficiency (EQE) of 50%. When **$PC_{61}BM$** was incorporated into **PPQ2T-BT-24**, a significantly shortened fall time of 8 ms along with a much-improved rise time of 1 ms were realized. These response times are among the best values reported for OPTs. The *R* and EQE of the devices using this polymer blend also increased to 0.88 A $W^{-1}$ and 189%, respectively.



Extensive research has been conducted on polymer semiconductors because of their certain desirable properties such as low manufacturing costs, light weight, mechanical flexibility, as well as low-temperature and solution processabilities.[1,2] These characteristics have led to studies of these materials for potential applications in optoelectronic devices such as organic light-emitting diodes (OLEDs),[3–5] organic photovoltaics (OPVs),[6–8] organic thin film transistors (OTFTs),[2,9,10] and organic phototransistors (OPTs),[11–13] which are a special type of OTFTs. Phototransistors (PTs) that respond in the region from the ultraviolet (UV) to near infrared (NIR) can be used for medical imaging, biological/chemical sensing, communication, environmental monitoring, and security.[12,14,15] Currently, most commercially available PTs are based on inorganic semiconductor materials such as silicon (Si), silicon carbide (SiC), gallium nitride (GaN), and indium gallium arsenide (InGaAs), which are known to have relatively narrow response spectral windows,[16,17] limiting their applications. Furthermore, it is difficult to fabricate large area PTs using inorganic materials due to their complicated fabrication processes.[18] The constrained spectral tunability and poor processability of inorganic semiconductor materials have inspired research into OPTs based on organic semiconductors because the organic semiconductors can be structurally readily tuned to obtain desired band gaps and allow facile device fabrication using solution based processing techniques such as printing.[12,19,20]

In terms of some device performance parameters, OPTs can be similar or even better than some inorganic PTs. For example, anthra[2,3-*b*]benzo[*d*]thiophene based devices displayed photoresponsivity (*R*) values as high as $\sim 10^3$ A $W^{-1}$,[21] outperforming that of single-crystal silicon phototransistors ($\sim$300 A $W^{-1}$).[22] Another important parameter is response time, which determines the operation frequency of a PT device when used as a photoelectrical switch (*e.g.* a silicon PT can achieve an operation frequency of $\sim 10^4$–$10^5$ Hz).[23] Some recently reported OPTs showed relatively short response times of $\sim$10's milliseconds (ms),[24–26] which are better than those of some inorganic PTs. However, most OPTs[27–30] show much longer response times (in seconds or longer) than that of a typical silicon PT ($\sim$5 μs).[23]

Pristine small molecule or polymer semiconductors have been extensively used as the charge transport and photoresponsive channel layers in OPTs. Recently, blending another photoactive component into the organic semiconductor matrix has been used to broaden the spectral coverage and bring about interesting photochemical properties to the OPTs. For example, photochromic small molecules such as spiropyran, diarylethene, and azobenzene have been used as additives in the blends, at the active layer/dielectric interface, and at the active layer/electrode interface to realize reversible photoresponse through photoisomerization of these molecules at different wavelengths.[31,32] In the more traditional sense the OTFTs operate under gate voltage control, but the OTFTs operation can also be modulated through optical/photochemical control.[33,34] More recently, blending small molecules and inorganic semiconductors with polymer semiconductors to form active layers with bulk heterojunction structures have also

[a] *Department of Chemical Engineering and Waterloo Institute of Nanotechnology (WIN), University of Waterloo, 200 University Ave West, Waterloo, N2L 3G1, Canada. E-mail: yuning.li@uwaterloo.ca; Fax: +1-519-888-4347; Tel: +1-519-888-4567 ext. 31105*

[b] *Department of Chemistry, Carleton University, Ottawa, ON, K1S 5B6, Canada*

† Electronic supplementary information (ESI) available: Experimental section and figures. See DOI: 10.1039/c7tc03023a

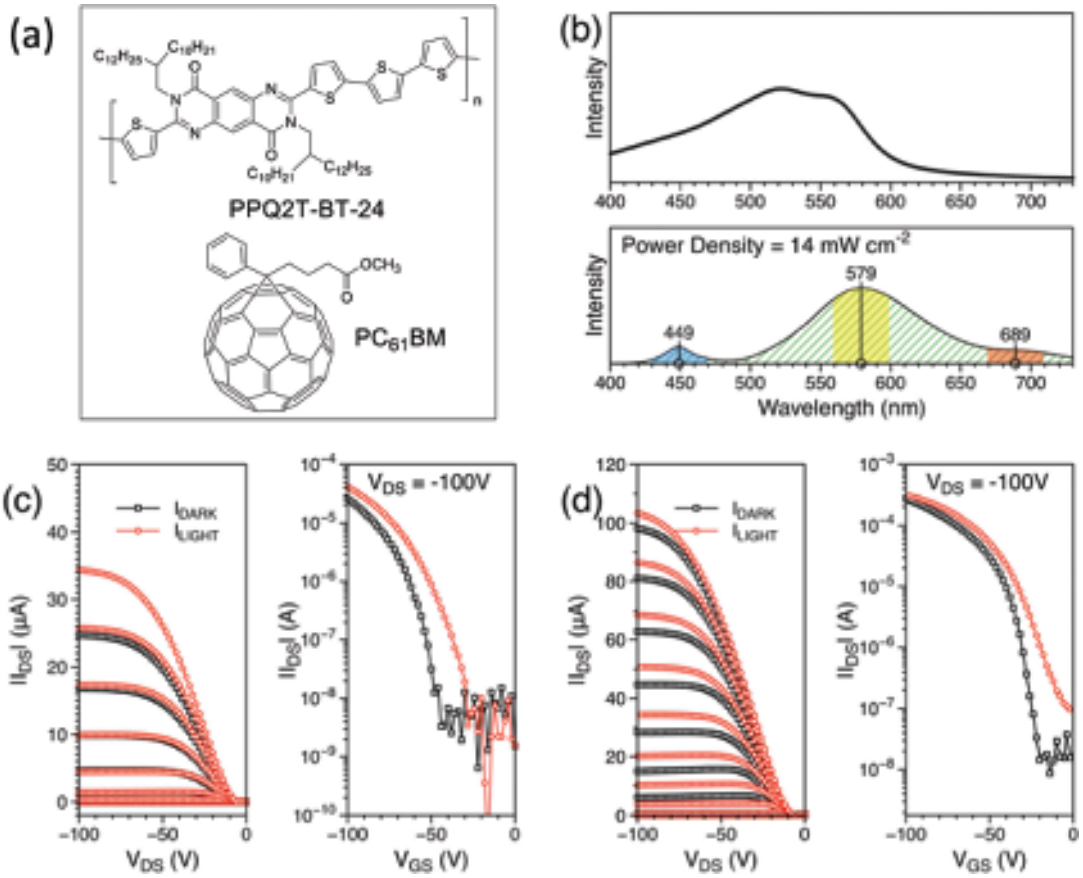


Fig. 1 Chemical structure of (a) **PPQ2T-BT-24** and **$PC_{61}BM$**. (b) The spectral analysis of the light source (bottom) with stacked overlaid UV-vis-NIR absorption profile of **PPQ2T-BT-24** thin film (top). (c and d) Output (left) and transfer (right) curves of **PPQ2T-BT-24** based (c) and **PPQ2T-BT-24**:**$PC_{61}BM$** based (d) OTFTs measured in the dark and illuminated at 14 mW $cm^{-2}$, respectively.

been studied with marked improvements in OPT performance when compared to their pristine counterparts.[18,35–39]

In this study, we report the phototransistor performance of a pyrimido[4,5-*g*]quinazoline-4,9-dione (PQ) based p-type polymer, **PPQ2T-BT-24** (Fig. 1a).[40] OPTs based on this polymer showed very short rise time ($T_R$) of 3 ms and fall time ($T_F$) of 59 ms. When an electron acceptor, phenyl-$C_{61}$-butyric acid methyl ester (**$PC_{61}BM$**), was added to **PPQ2T-BT-24** (at a 1 : 1 weight ratio), the $T_F$ of the **PPQ2T-BT-24**:**$PC_{61}BM$** blend was remarkably shortened to 8 ms. At the same time, the $T_R$ was also reduced to a very low value of 1 ms. These response times are among the best values reported so far for OPTs.

To measure the transient photocurrent responses, a 10 W LED (with a power density of 14 mW $cm^{-2}$) with a color temperature of 3000 to 3500 K with an emission peak at 579 nm (Fig. 1b bottom) was utilized, which overlaps with the absorption profile of **PPQ2T-BT-24** which has a $\lambda_{max}$ at 562 nm (Fig. 1b top).[40] The typical output and transfer characteristics of the devices based on this polymer in the absence of light (black) and under illumination (red) are shown in Fig. 1c. The output curves were swept between 0 V and −100 V for drain voltage ($V_{DS}$), while gate voltage ($V_{GS}$) was held constant at values chosen from 0 V to −100 V with 10 V increments. For all devices, there was an increase in drain current ($I_{DS}$) under illumination compared with their corresponding devices measured in dark. The $I_{DS}$ for the transfer curves, where $V_{DS}$ was held constant at −100 V and $V_{GS}$ was swept from 20 to −100 V, also increased under illumination compared to those in dark. The OTFT devices measured in dark showed typical p-type

Table 1 Summary of OTFT characteristics in dark at 200 °C annealed. Transient photocurrent response times for rise and fall and the utmost photoresponsivity ($R$) and external quantum efficiency (EQE) achieved

| | | | | Response time [ms] | | | | |
|---|---|---|---|---|---|---|---|---|
| Channel layer | $\mu^a$ [$\times 10^{-3}$ $cm^2$ $V^{-1}$ $s^{-1}$] | $V_{TH}$ [V] | $I_{ON}/I_{OFF}$ | Rise time ($T_R$) | Fall time ($T_F$) | $R$ [A $W^{-1}$] | $P$ | EQE [%] |
| **PPQ2T-BT-24** | 3.95 (3.90 ± 0.06) | −53.1 | $\sim 10^5$ | 3 | 59 | 0.24 | $1.02 \times 10^2$ | 50 |
| **PPQ2T-BT-24:$PC_{61}BM$** | 19.22 (16.88 ± 1.32) | −25.3 | $\sim 10^5$ | 1 | 8 | 0.88 | $0.74 \times 10^2$ | 189 |

[a] Average and standard deviation of 5 devices.

semiconductor characteristics with hole mobilities in the order of $10^{-3}$ $cm^2$ $V^{-1}$ $s^{-1}$ (in Table 1), which are comparable with our previously reported values for this polymer.[31]

The transient photocurrent responses of OPTs over time are shown in Fig. 2a, where the devices were measured under illumination (on-state) for a 5 s interval, followed by a 12 s interval without illumination (off-state). The response times, $T_R$ and $T_F$, were measured at constant $V_{DS}$ and $V_{GS}$ values of −100 V. The $T_R$ is defined as the time required for the $I_{DS}$ to increase from 10% to 90% of its maximum light on-state value, while the $T_F$ is defined as the time required for the $I_{DS}$ to drop to its 90% since the light source is turned off.[42] **PPQ2T-BT-24** demonstrated a $T_R$ of 3 ms and a $T_F$ of 59 ms (Fig. 2b). This $T_R$ is shorter than those of many previously reported polymer-based OPTs[25,26,30,35] and is nearly 4-fold shorter than the reported rise times for some inorganic photodetectors.[43,44]

The other important parameter for OPTs, photoresponsivity ($R$), was calculated using the following equation ($R = I_{ill} - I_{dark}/AP_{inc}$)[24–26] where $I_{ill}$ and $I_{dark}$ are defined as $I_{DS}$ under illumination and in the dark, respectively, $A$ is the channel area, and $P_{inc}$ is the power density of incident light. Fig. 2d shows the plot of $R$ as a function of $V_{GS}$, which ranges from 20 to −100 V, while the $V_{DS}$ was kept constant at −100 V. The $R$ values of the devices are negligible when the $V_{GS}$ was in the range between 20 and −20 V; however, the $R$ values improved greatly as the $V_{GS}$ increased further in the negative direction. At $V_{GS}$ = −100 V, an $R$ value of 0.24 A $W^{-1}$ was achieved, which is greater than those of some previously reported OPTs.[26,45] The photocurrent/dark-current ratio ($P = (I_{ill} - I_{dark})/I_{dark}$) reached $1.02 \times 10^2$ at $V_{GS}$ = −44 V.

An analogous parameter to $R$ is the external quantum efficiency (EQE or $\eta$), which is defined as the ratio of generated carriers to incident photons in the transistor channel area. The EQE values can be calculated by using the equation ($EQE = Rhc/\lambda_{peak}e$)[46] where $R$ is defined previously, $h$ is Planck's constant ($6.62607 \times 10^{-34}$ $m^2$ kg $s^{-1}$), $c$ is the speed of light in vacuum, $e$ is the elementary charge ($1.60218 \times 10^{-19}$ C), and $\lambda_{peak}$ is the wavelength of incident light with maximum intensity. For the convenience of EQE calculation, the LED light source was assumed to be monochromatic with a $\lambda_{peak}$ of 579 nm, similar to the method adopted by Labram *et al.*[37] The OPTs with **PPQ2T-BT-24** showed an EQE of up to 50% (Fig. 2d).

Incorporating a fullerene derivative (an n-type semiconductor), such as **$PC_{61}BM$** (Fig. 1a), into a p-type organic semiconductor to form a bulk-heterojunction structure has been reported to be able to improve the OPT performance[35,42,47] by improving the efficiency of photoinduced charge generation.[48] Therefore, **$PC_{61}BM$** was

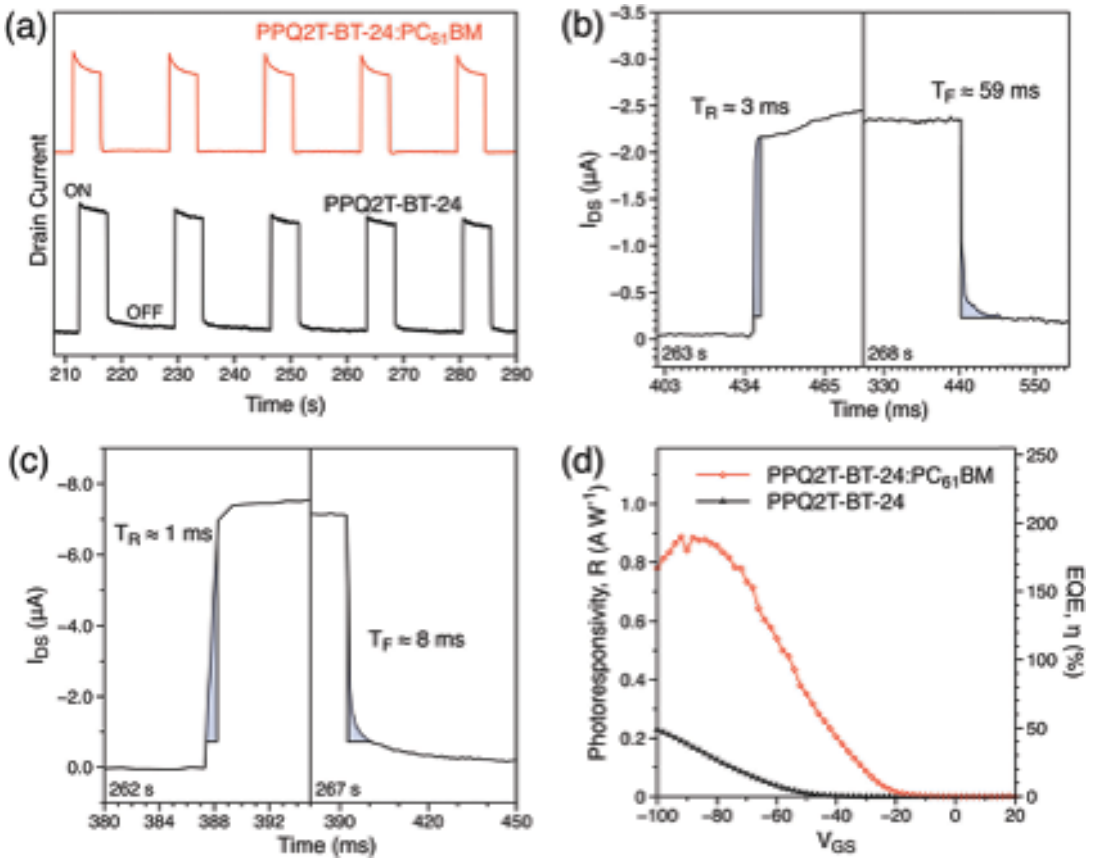


Fig. 2 Transient photocurrent responses of (a) **PPQ2T-BT-24** and **PPQ2T-BT-24**:**$PC_{61}BM$** as a function of time in response to illumination at 14 mW $cm^{-2}$ with 5 s illumination on-state followed by 12 s illumination off-state (dark). (b and c) The estimated rise ($T_R$) and fall ($T_F$) time of **PPQ2T-BT-24** and **PPQ2T-BT-24**:**$PC_{61}BM$** based devices, respectively. Data collected at 1 ms intervals. (d) The photoresponsivity ($R$) and external quantum efficiency (EQE, $\eta$) of **PPQ2T-BT-24** and **PPQ2T-BT-24**:**$PC_{61}BM$** based devices at a constant $V_{DS}$ of −100 V.

blended with **PPQ2T-BT-24** at a polymer : **$PC_{61}BM$** ratio of 1 : 1 (weight ratio) in order to improve the OPT performance (Fig. 1d). In comparison to pristine **PPQ2T-BT-24**, the **PPQ2T-BT-24:$PC_{61}BM$** blend showed dramatic increases in the $I_{DS}$ together with enhanced mobilities of up to 0.019 $cm^2\ V^{-1}\ s^{-1}$ (Fig. 1d and Table 1). This mobility enhancement is most likely due to the significantly improved crystallinity of the blend film (to be discussed later). The $T_R$ of the OPTs with this polymer blend decreased to 1 ms (Fig. 2a and c). The $T_F$ was shortened dramatically to 8 ms, which is an order magnitude lower compared to the pristine polymer. These values are superior to those of some inorganic and hybrid materials based phototransistors[35,43,44,49–53] and are among the best for small molecule,[28–30,46,54] polymer,[25–27,55–60] and polymer blend[61] based phototransistors. Additionally, the EQE values were improved to 189%. Compared to a photodiode, which has a maximum EQE of 100%, a phototransistor can realize an EQE greater than 100% likely due to the photo-multiplication phenomenon enabled by the field-induced tunneling as well as the nature of the semiconductor layer.[62,63] The maximum EQE value was attained at a lower $V_{GS}$ ($\sim -85$ V shown in Fig. 2d) in comparison to that of the pristine polymer (at $V_{GS} = \sim -100$ V). This observation may be attributed to the photo-induced shift of $V_{TH}$ due to the photovoltaic effect[64] and an oversaturation behavior in the $I_{DS}$.[65] The photovoltaic effect, where the generated electron–hole pairs (or excitons) dissociate into electrons and holes (Fig. 3), which drift as polarons in opposing directions under a source–drain bias, contributes to the increased $I_{DS}$ and EQE.[65] In the case of p-type semiconductors, holes flow to the drain contact whereas the electrons accumulate at the source contact where they effectively lower the injection barrier for holes.

The lowered hole injection barrier results in a decrease in contact resistance with a positive shift of $V_{TH}$ (or a reduction in $|V_{TH}|$) thereby increasing $I_{DS}$.[12] The **$PC_{61}BM$** domains in the blend would facilitate the electron transport (*i.e.* movement of electrons towards the source contact) and increase photocurrent[35] and thus their accumulation at the source. The lowered hole injection barrier due to the accumulation of electrons at the source might also have contributed to the afore-mentioned photo-multiplication phenomenon. On the contrary, large polaron densities resulting from a change in the power density (*i.e.* increasing power densities of the light source) can increase the chance of recombining polarons, which reduces the $I_{DS}$ and hence the $R$ and EQE values.[65] If the power density remains constant and large biases are applied, a similar phenomenon may occur.[42,66–69] At a higher $V_{GS}$, a larger amount of charge carriers (in this case holes) are injected, producing an excess of holes, which can cross-recombine with the electrons in the polarons. Both of these situations result in attenuated contributions to $I_{DS}$ and as a result, ''oversaturation'' may occur, where the increased portion in $I_{DS}$ caused by the photovoltaic effect slows down and eventually stagnates (saturated), which results in a decrease in EQE and $R$. For OPTs with the pristine **PPQ2T-BT-24**, dissociation of photo-generated excitons is less efficient (compared to the blend) where the cross-recombination effect is minimal. Therefore, a monotonic increase in EQE and $I_{DS}$ with $V_{GS}$ is observed for OPT devices based on the pristine **PPQ2T-BT-24**. With the addition of **$PC_{61}BM$** to the polymer, the exciton dissociation is facilitated at the donor (polymer) and acceptor (**$PC_{61}BM$**) interface, which is well known for OPV devices.[16,70,71] Therefore, a greater number of photo-generated holes and electrons exist in the blend channel layer of the OPTs compared

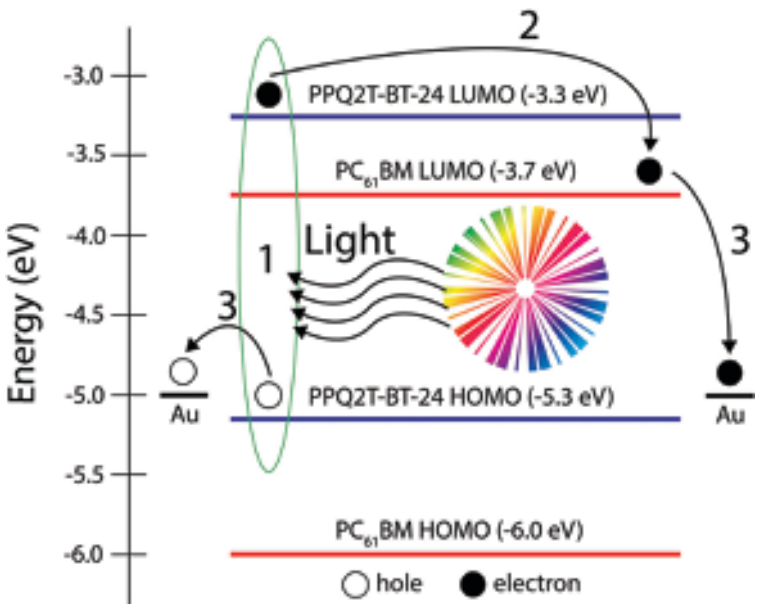


Fig. 3 The energy band diagram of the **PPQ2T-BT-24**:**$PC_{61}BM$** based devices showing exciton generation (1), the dissociation of the exciton into electron and hole (2), and the drifting of hole and electron towards the gold (Au) drain and source electrodes, respectively (3). For simplicity, the charges which are generated by the field effect are not illustrated. The HOMO and LUMO energy levels of **$PC_{61}BM$** and **PPQ2T-BT-24** were taken from ref. 41 and of ref. 40, respectively.

 

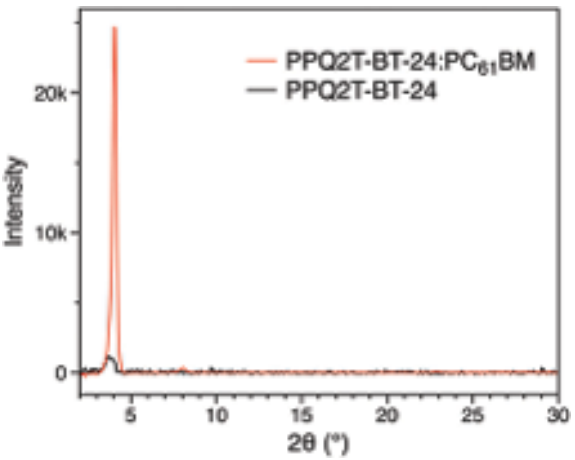


Fig. 4 XRD patterns of pristine polymer **PPQ2T-BT-24** and **PPQ2T-BT-24**:**PC$_{61}$BM** of 200 °C-annealed thin films.

with the pristine polymer based devices at high $V_{GS}$. Consequently, the cross-recombination effect becomes significant and the "over-saturation" occurs, *i.e.*, an optimum $V_{GS}$ was observed. The maximum $R$ of the OPT devices based on the polymer blend increased to 0.88 A W$^{-1}$. The maximum $P$ value is $0.74 \times 10^2$ at $V_{GS} = -20$ V. Overall, the OPTs based on the **PPQ2T-BT-24** and its blend with **PC$_{61}$BM** showed excellent response times and moderate $R$ and $P$ values compared to OPTs with other polymers and polymer blends reported previously (Table S1, ESI†).

Interestingly, it was noticed that the hole mobility (up to $1.92 \times 10^{-2}$ cm$^2$ V$^{-1}$ s$^{-1}$) of the polymer blend increased by an order of magnitude compared to the pristine polymer (up to $3.95 \times 10^{-3}$ cm$^2$ V$^{-1}$ s$^{-1}$) when the OTFTs were measured in the dark (Table 1). To investigate the cause for the improved mobility, XRD and AFM were used to probe the molecular ordering and morphologies of the blend and the pristine polymer. The XRD patterns for the polymer blend showed a dramatic increase in crystallinity in comparison to the pristine polymer (Fig. 4), which can be attributed to the antiplasticization effects[72,73] of **PC$_{61}$BM**. AFM height images of the 200 °C-annealed thin film (Fig. S1, ESI†) indicated that the pristine polymer film was quite smooth with a root-mean-square (RMS) roughness of 0.23 nm. On the other hand, the polymer blend displayed large aggregates with a much larger RMS roughness of 81.0 nm, most likely due to the very high crystallinity of the polymer in the blend as verified by the XRD measurement as well as the aggregation of **PC$_{61}$BM** due to the relatively poor solubility of **PC$_{61}$BM** and the rapid evaporation of the low boiling point solvent used (chloroform).

The improved mobility of the polymer blend may also account for their improved response times and photoresponsivities. However, the exact effects of mobility on the response times and photoresponsivities are still unclear. In retrospect, although **PPQ2T-BT-24** showed relatively low mobility of $\sim 10^{-3}$ cm$^2$ V$^{-1}$ s$^{-1}$, it demonstrated very short response times in OPTs compared to the previously reported organic semiconductor materials with much higher mobilities.[29,30,39,46,54,74,75] Therefore, it seems that the PQ building block might be especially beneficial for achieving short response times. The origin for the short response times observed for this PQ polymer will be the subject of our next step investigation.

## Conclusions

In conclusion, the pyrimido[4,5-*g*]quinazoline-4,9-dione (PQ) based polymer, **PPQ2T-BT-24**, was studied as an active channel layer in organic phototransistors. The devices using the pristine **PPQ2T-BT-24** exhibited an $R$ of 0.24 A W$^{-1}$, a very short $T_R$ of 3 ms, a $T_F$ of 59 ms, and an EQE of 50%. By blending **PC$_{61}$BM** with this polymer, the **PPQ2T-BT-24 : PC$_{61}$BM** blend (at a 1 : 1 weight ratio) showed much improved OPT performance with an $R$ of 0.88 A W$^{-1}$, a $T_R$ of 1 ms, a $T_F$ of 8 ms, and an EQE of 189%. These results demonstrated that PQ-based polymers are very promising for high performance, particularly fast switching, OPT devices.

## Conflicts of interest

There are no conflicts to declare.

## Acknowledgements

Financial support of this work by the Natural Sciences and Engineering Research Council (NSERC) of Canada (Discovery Grant # RGPIN-2016-04366) is acknowledged.

## Notes and references

1 A. R. Murphy and J. M. Frechet, *Chem. Rev.*, 2007, **107**, 1066–1096.
2 C. Wang, H. Dong, W. Hu, Y. Liu and D. Zhu, *Chem. Rev.*, 2012, **112**, 2208–2267.
3 R. H. Friend, R. W. Gymer, A. B. Holmes, J. H. Burroughes, R. N. Marks, C. Taliani, D. D. C. Bradley, D. A. Dos Santos, J. L. Bredas, M. Logdlund and W. R. Salaneck, *Nature*, 1999, **397**, 121–128.
4 A. P. Kulkarni, C. J. Tonzola, A. Babel and S. A. Jenekhe, *Chem. Mater.*, 2004, **16**, 4556–4573.
5 A. C. Grimsdale, K. L. Chan, R. E. Martin, P. G. Jokisz and A. B. Holmes, *Chem. Rev.*, 2009, **109**, 897–1091.
6 E. Bundgaard and F. C. Krebs, *Sol. Energy Mater. Sol. Cells*, 2007, **91**, 954–985.
7 L. Dou, J. You, Z. Hong, Z. Xu, G. Li, R. A. Street and Y. Yang, *Adv. Mater.*, 2013, **25**, 6642–6671.
8 A. J. Heeger, *Adv. Mater.*, 2014, **26**, 10–27.
9 C. D. Dimitrakopoulos and P. R. L. Malenfant, *Adv. Mater.*, 2002, **14**, 99–117.
10 H. Klauk, *Chem. Soc. Rev.*, 2010, **39**, 2643–2666.
11 H. Dong, H. Zhu, Q. Meng, X. Gong and W. Hu, *Chem. Soc. Rev.*, 2012, **41**, 1754–1808.
12 K. J. Baeg, M. Binda, D. Natali, M. Caironi and Y. Y. Noh, *Adv. Mater.*, 2013, **25**, 4267–4295.
13 P. C. Gu, Y. F. Yao, L. L. Feng, S. J. Niu and H. L. Dong, *Polym. Chem.*, 2015, **6**, 7933–7944.
14 A. Rogalski, J. Antoszewski and L. Faraone, *J. Appl. Phys.*, 2009, **105**, 091101.

15 E. H. Sargent, *Adv. Mater.*, 2005, **17**, 515–522.
16 L. L. Du, X. Luo, F. Y. Zhao, W. L. Lv, J. P. Zhang, Y. Q. Peng, Y. Tang and Y. Wang, *Carbon*, 2016, **96**, 685–694.
17 X. Luo, L. L. Du, W. L. Lv, L. Sun, Y. Li, Y. Q. Peng, F. Y. Zhao, J. P. Zhang, Y. Tang and Y. Wang, *Synth. Met.*, 2015, **210**, 230–235.
18 H. Hwang, H. Kim, S. Nam, D. D. Bradley, C. S. Ha and Y. Kim, *Nanoscale*, 2011, **3**, 2275–2279.
19 Y. Liu, H. F. Wang, H. L. Dong, J. H. Tan, W. P. Hu and X. W. Zhan, *Macromolecules*, 2012, **45**, 1296–1302.
20 Y. S. Kim, S. Y. Bae, K. H. Kim, T. W. Lee, J. A. Hur, M. H. Hoang, M. J. Cho, S. J. Kim, Y. Kim, M. Kim, K. Lee, S. J. Lee and D. H. Choi, *Chem. Commun.*, 2011, **47**, 8907–8909.
21 Y. L. Guo, C. Y. Du, C. A. Di, J. Zheng, X. N. Sun, Y. G. Wen, L. Zhang, W. P. Wu, G. Yu and Y. Q. Liu, *Appl. Phys. Lett.*, 2009, **94**, 143303.
22 N. M. Johnson and A. Chiang, *Appl. Phys. Lett.*, 1984, **45**, 1102–1104.
23 C. Bingruo, G. Fanrong and W. Biao, *Wuhan Univ. J. Nat. Sci.*, 1997, **2**, 431–434.
24 B. Mukherjee, M. Mukherjee, Y. Choi and S. Pyo, *J. Phys. Chem. C*, 2009, **113**, 18870–18873.
25 S. Dutta and K. S. Narayan, *Synth. Met.*, 2004, **146**, 321–324.
26 Q. H. Wang, M. Zhu, D. Wu, G. B. Zhang, X. H. Wang, H. B. Lu, X. H. Wang and L. Z. Qiu, *J. Mater. Chem. C*, 2015, **3**, 10734–10741.
27 H. L. Dong, H. X. Li, E. J. Wang, H. Nakashima, K. Torimitsu and W. P. Hu, *J. Phys. Chem. C*, 2008, **112**, 19690–19693.
28 T. P. I. Saragi, R. Pudzich, T. Fuhrmann and J. Salbeck, *Appl. Phys. Lett.*, 2004, **84**, 2334–2336.
29 K. H. Kim, S. Y. Bae, Y. S. Kim, J. A. Hur, M. H. Hoang, T. W. Lee, M. J. Cho, Y. Kim, M. Kim, J. I. Jin, S. J. Kim, K. Lee, S. J. Lee and D. H. Choi, *Adv. Mater.*, 2011, **23**, 3095–3099.
30 B. Lucas, A. El Amrani, M. Chakaroun, B. Ratier, R. Antony and A. Moliton, *Thin Solid Films*, 2009, **517**, 6280–6282.
31 Y. Wakayama, R. Hayakawa and H. S. Seo, *Sci. Technol. Adv. Mater.*, 2014, **15**, 024202.
32 L.-N. Fu, B. Leng, Y.-S. Li and X.-K. Gao, *Chin. Chem. Lett.*, 2016, **27**, 1319–1329.
33 C. Raimondo, N. Crivillers, F. Reinders, F. Sander, M. Mayor and P. Samori, *Proc. Natl. Acad. Sci. U. S. A.*, 2012, **109**, 12375–12380.
34 M. E. Gemayel, K. Borjesson, M. Herder, D. T. Duong, J. A. Hutchison, C. Ruzie, G. Schweicher, A. Salleo, Y. Geerts, S. Hecht, E. Orgiu and P. Samori, *Nat. Commun.*, 2015, **6**, 6330.
35 H. Xu, J. Li, B. H. Leung, C. C. Poon, B. S. Ong, Y. Zhang and N. Zhao, *Nanoscale*, 2013, **5**, 11850–11855.
36 S. Nam, J. Seo, S. Park, S. Lee, J. Jeong, H. Lee, H. Kim and Y. Kim, *ACS Appl. Mater. Interfaces*, 2013, **5**, 1385–1392.
37 H. Han, S. Nam, J. Seo, C. Lee, H. Kim, D. D. Bradley, C. S. Ha and Y. Kim, *Sci. Rep.*, 2015, **5**, 16457.
38 H. Hyemi, N. Sungho, S. Jooyeok, J. Jaehoon, K. Hwajeong, D. D. C. Bradley and K. Youngkyoo, *IEEE J. Sel. Top. Quantum Electron.*, 2016, **22**, 147–153.
39 D. Ljubic, C. S. Smithson, Y. Wu and S. Zhu, *ACS Appl. Mater. Interfaces*, 2016, **8**, 3744–3754.
40 J. Quinn, C. Guo, B. Sun, A. Chan, Y. He, E. Jin and Y. Li, *J. Mater. Chem. C*, 2015, **3**, 11937–11944.
41 M. Yasin, T. Tauqeer, K. S. Karimov, S. E. San, A. Kosemen, Y. Yerli and A. V. Tunc, *Microelectron. Eng.*, 2014, **130**, 13–17.
42 Z. Qi, J. M. Cao, H. Li, L. M. Ding and J. Z. Wang, *Adv. Funct. Mater.*, 2015, **25**, 3138–3146.
43 P. G. Hu, J. Zhang, M. N. Yoon, X. F. Qiao, X. Zhang, W. Feng, P. H. Tan, W. Zheng, J. J. Liu, X. N. Wang, J. C. Idrobo, D. B. Geohegan and K. Xiao, *Nano Res.*, 2014, **7**, 694–703.
44 Z. Wang, M. Safdar, C. Jiang and J. He, *Nano Lett.*, 2012, **12**, 4715–4721.
45 G. B. Zhang, J. H. Guo, J. Zhang, W. T. Li, X. H. Wang, H. B. Lu and L. Z. Qiu, *Dyes Pigm.*, 2016, **126**, 20–28.
46 J. G. Labram, P. H. Wobkenberg, D. D. C. Bradley and T. D. Anthopoulos, *Org. Electron.*, 2010, **11**, 1250–1254.
47 T. D. Anthopoulos, *Appl. Phys. Lett.*, 2007, **91**, 113513.
48 C. H. Lee, G. Yu, D. Moses, K. Pakbaz, C. Zhang, N. S. Sariciftci, A. J. Heeger and F. Wudl, *Phys. Rev. B: Condens. Matter Mater. Phys.*, 1993, **48**, 15425–15433.
49 H. Liu, Q. Sun, J. Xing, Z. Zheng, Z. Zhang, Z. Lu and K. Zhao, *ACS Appl. Mater. Interfaces*, 2015, **7**, 6645–6651.
50 F. Yan, J. H. Li and S. M. Mok, *J. Appl. Phys.*, 2009, **106**, 074501.
51 X. Fan, X. M. Meng, X. H. Zhang, M. L. Zhang, J. S. Jie, W. J. Zhang, C. S. Lee and S. T. Lee, *J. Phys. Chem. C*, 2009, **113**, 834–838.
52 J. Zhou, Y. Gu, Y. Hu, W. Mai, P. H. Yeh, G. Bao, A. K. Sood, D. L. Polla and Z. L. Wang, *Appl. Phys. Lett.*, 2009, **94**, 191103.
53 Y. Hu, J. Zhou, P. H. Yeh, Z. Li, T. Y. Wei and Z. L. Wang, *Adv. Mater.*, 2010, **22**, 3327–3332.
54 M. Y. Cho, S. J. Kim, Y. D. Han, D. H. Park, K. H. Kim, D. H. Choi and J. Joo, *Adv. Funct. Mater.*, 2008, **18**, 2905–2912.
55 H. J. Nam, J. Cha, S. H. Lee, W. J. Yoo and D. Y. Jung, *Chem. Commun.*, 2014, **50**, 1458–1461.
56 L. R. Fleet, J. Stott, B. Villis, S. Din, M. Serri, G. Aeppli, S. Heutz and A. Nathan, *ACS Appl. Mater. Interfaces*, 2017, **9**, 20686–20695.
57 Y. Lei, N. Li, W.-K. E. Chan, B. S. Ong and F. Zhu, *Org. Electron.*, 2017, **48**, 12–18.
58 M. J. Kim, S. Choi, M. Lee, H. Heo, Y. Lee, J. H. Cho and B. Kim, *ACS Appl. Mater. Interfaces*, 2017, **9**, 19011–19020.
59 X. Liu, Y. Guo, Y. Ma, H. Chen, Z. Mao, H. Wang, G. Yu and Y. Liu, *Adv. Mater.*, 2014, **26**, 3631–3636.
60 M. Kim, H.-J. Ha, H.-J. Yun, I.-K. You, K.-J. Baeg, Y.-H. Kim and B.-K. Ju, *Org. Electron.*, 2014, **15**, 2677–2684.
61 M. Zhu, S. Lv, Q. Wang, G. Zhang, H. Lu and L. Qiu, *Nanoscale*, 2016, **8**, 7738–7748.
62 L. Zhang, T. Wu, Y. Guo, Y. Zhao, X. Sun, Y. Wen, G. Yu and Y. Liu, *Sci. Rep.*, 2013, **3**, 1080.
63 R. M. Pinto, W. Gouveia, A. I. S. Neves and H. Alves, *Appl. Phys. Lett.*, 2015, **107**, 223301.
64 H. S. Kang, C. S. Choi, W. Y. Choi, D. H. Kim and K. S. Seo, *Appl. Phys. Lett.*, 2004, **84**, 3780–3782.

 

65 K. Wasapinyokul, W. I. Milne and D. P. Chu, *J. Appl. Phys.*, 2009, **105**, 024509.
66 L. C. Ma, Z. R. Yi, S. Wang, Y. Q. Liu and X. W. Zhan, *J. Mater. Chem. C*, 2015, **3**, 1942–1948.
67 W. F. Jin, Z. W. Gao, Y. Zhou, B. Yu, H. Zhang, H. L. Peng, Z. F. Liu and L. Dai, *J. Mater. Chem. C*, 2014, **2**, 1592–1596.
68 Y. Liu, Q. Q. Shi, L. C. Ma, H. L. Dong, J. H. Tan, W. P. Hu and X. W. Zhan, *J. Mater. Chem. C*, 2014, **2**, 9505–9511.
69 M. C. Hamilton, S. Martin and J. Kanicki, *IEEE Trans. Electron Devices*, 2004, **51**, 877–885.
70 R. S. Bhatta and M. Tsige, *ACS Appl. Mater. Interfaces*, 2014, **6**, 15889–15896.
71 C. F. N. Marchiori and M. Koehler, *Synth. Met.*, 2010, **160**, 643–650.
72 B. Sun, W. Hong, H. Aziz, N. M. Abukhdeir and Y. N. Li, *J. Mater. Chem. C*, 2013, **1**, 4423–4426.
73 L. Murphy, B. Sun, W. Hong, H. Aziz and Y. N. Li, *Aust. J. Chem.*, 2015, **68**, 1741–1749.
74 C. S. Smithson, D. Ljubic, Y. Wu and S. Zhu, *J. Mater. Chem. C*, 2015, **3**, 8090–8096.
75 F. Loffredo, A. Bruno, A. D. Del Mauro, I. A. Grimaldi, R. Miscioscia, G. Nenna, G. Pandolfi, M. Petrosino, F. Villani, C. Minarini and A. Facchetti, *Phys. Status Solidi A*, 2014, **211**, 460–466.